NEOPLASIA
www.neoplasia.com

Volume 17 Number 4 April 2015 pp. 374–384 374

Macrophage Ablation Reduces M2-Like Populations and Jeopardizes Tumor Growth in a MAFIA-Based Glioma Model[1,2]

Konrad Gabrusiewicz*, Mohammad B. Hossain*, Nahir Cortes-Santiago*, Xuejun Fan*, Bozena Kaminska†, Frank C. Marini‡, Juan Fueyo*,§ and Candelaria Gomez-Manzano*,¶

*Department of Neuro-Oncology, The University of Texas MD Anderson Cancer Center, Houston, TX, USA; †Nencki Institute of Experimental Biology, Polish Academy of Sciences, Warsaw, Poland; ‡Comprehensive Cancer Center, Wake Forest University, Winston-Salem, NC, USA; §Department of Neurosurgery, The University of Texas MD Anderson Cancer Center, Houston, TX, USA; ¶Department of Genetics, The University of Texas MD Anderson Cancer Center, Houston, TX, USA

Abstract

Monocytes/macrophages are an influential component of the glioma microenvironment. However, understanding their diversity and plasticity constitute one of the most challenging areas of research due to the paucity of models to study these cells' inherent complexity. Herein, we analyzed the role of monocytes/macrophages in glioma growth by using a transgenic model that allows for conditional ablation of this cell population. We modeled glioma using intracranial GL261-bearing CSF-1R–GFP$^+$ macrophage Fas-induced apoptosis (MAFIA) transgenic mice. Conditional macrophage ablation was achieved by exposure to the dimerizer AP20187. Double immunofluorescence was used to characterize M1- and M2-like monocytes/macrophages during tumor growth and after conditional ablation. During glioma growth, the monocyte/macrophage population consisted predominantly of M2 macrophages. Conditional temporal depletion of macrophages reduced the number of GFP$^+$ cells, targeting mainly the repopulation of M2-polarized cells, and altered the appearance of M1-like monocytes/macrophages, which suggested a shift in the M1/M2 macrophage balance. Of interest, compared with control-treated mice, macrophage-depleted mice had a lower tumor mitotic index, microvascular density, and reduced tumor growth. These results demonstrated the possibility of studying *in vivo* the role and phenotype of macrophages in gliomas and suggested that transitory depletion of CSF-1R$^+$ population influences the reconstitutive phenotypic pool of these cells, ultimately suppressing tumor growth. The MAFIA model provides a much needed advance in defining the role of macrophages in gliomas.

Neoplasia (2015) 17, 374–384

Introduction

Cells of the monocyte/macrophage lineage are considered key components of the tumor microenvironment that operate in conflicting ways as tumor-antagonizing or tumor-promoting inflammatory cells [1,2]. Thus, tumor-associated macrophages (TAMs) are characterized by their diversity and plasticity, which can undergo two polarization states that represent extremes of a continuum: the classically activated M1 (proinflammatory) and the alternatively activated M2-like (tumor promoting) phenotypes [3]. Studies of several types of human solid tumors, including gliomas, have resulted in controversial findings regarding the correlation of the presence of TAMs and prognosis [4–7]. Functional studies aiming to deplete

Address all correspondence to: Candelaria Gomez-Manzano, MD, Departments of Neuro-Oncology and Genetics, The University of Texas MD Anderson Cancer Center, Houston, TX 77030, USA.
E-mail: cmanzano@mdanderson.org

[1] This study was supported by the National Institute of Health (R01 NS069964), the Concern Foundation, the Rosalie B. Hite Fellowship, and the National Cancer Institute Institutional Core grant (CA16672; Research Animal Support Facility at The University of Texas MD Anderson Cancer).
[2] This article refers to supplementary materials, which are designated by Figures W1 to W4 and are available online at www.neoplasia.com.
Received 21 October 2014; Revised 10 March 2015; Accepted 18 March 2015

1476-5586/15
http://dx.doi.org/10.1016/j.neo.2015.03.003

macrophages in glioma animal models have not explained these discrepancies and described macrophages as having either a positive or a negative influence on tumor growth [8,9].

Modeling the tumor microenvironment is one of the most challenging areas of research due to the paucity of models for studying its inherent complexity. In this work, we took advantage of a previously generated transgenic model that allows conditional and temporal ablation of the macrophage population [10]. The macrophage Fas-induced apoptosis (MAFIA) transgenic mouse model has been previously validated in studies on the role of macrophages in bone marrow homeostasis [11–13] and in several pathogenic diseases [14,15]. In this model, a murine *c-fms* promoter induces the expression of a transgene containing enhanced green fluorescent protein (EGFP) and a suicide fusion protein made up of the FK506-binding protein and the cytoplasmic domain of Fas. Expressed on cells of the mononuclear phagocyte system in the mouse, *c-fms* encodes the receptor for macrophage colony-stimulating factor (CSF-1) [16]. CSF-1R is known to be expressed in monocytes, tissue macrophages, and monocyte-derived dendritic cells [17]. Specifically, in the MAFIA brain tissue, EGFP is detectable in macrophages associated with the microvasculature and meningeal surfaces and in microglia [16]. Systemic administration of AP20187 dimerizes the suicide protein, inducing Fas-mediated apoptosis through activation of the caspase-8 pathway in myeloid lineage cells (i.e., macrophages and dendritic cells) and ultimately reducing the number of $EGFP^+$ cells by more than 90% in bone marrow and peritoneum and more than 70% in blood and in spleen, lung, and thymus tissue [10]. The use of this model in cancer has so far been limited to two recent studies on metastasis of B16-F10 melanoma [18] and in combination with a preneoplastic progression model for breast cancer [19].

In this study, we analyzed the kinetics of intracranial syngeneic murine GL261 cells by using the MAFIA mouse model to allow for easy identification and conditional ablation of the tumor-associated myeloid population. Our study unequivocally demonstrated the role of $CSFR\text{-}1R^+$ myeloid population in tumor proliferation, angiogenesis, and growth at different stages of tumor development. In addition, we show a switch in the M2/M1 polarization status that accompanies the repopulation of TAMs on conditional myeloid ablation. Finally, the work presented here sets up the basis for further studies on the pathobiology of macrophages and drug testing for malignant glioma treatments.

Materials and Methods

Cell Culture and In Vitro Studies

Murine GL261 glioma cells and the RAW 264.7 macrophage cell line were obtained from the Developmental Therapeutics Program (DTP), Division of Cancer Treatment and Diagnosis (DCTD) Tumor Repository (National Institutes of Health (NIH), Frederick, MD) and American Type Culture Collection (ATCC), Manassas, Virginia, respectively, and cultured in Dulbecco's modified Eagle's medium (Cellgro) with 10% FBS (Cellgro) and antibiotics (50 U/ml penicillin and 50 μg/ml streptomycin) in a humidified atmosphere of CO_2/air (5%/95%) at 37°C.

For macrophage polarization, RAW 264.7 cells were cultured in complete medium and stimulated for 24 hours with 1 ng/ml lipopolysaccharides from *Escherichia coli* 055:B5 (Sigma, St. Louis, Missouri) and 10 IU/ml Interferon gamma (IFN-γ) (Peprotech, Rocky Hill, New Jersey) for M1 or 20 ng/ml Interleukin 4 (IL-4) (R&D Systems, Minneapolis, Minnesota) for M2 activation.

GL261 and RAW 264.7 cell lines were treated with AP20187 with different concentrations (0.01, 0.1, 1, and 10 nM) or vehicle for 24 or 48 hours, and cell proliferation was measured using CyQUANT Direct Cell Proliferation Assay Kit (Life Technologies, Grand Island, New York) according the manufacturer's protocol.

Real-Time Polymerase Chain Reaction Array

Total RNA was extracted from RAW 264.7 and M1- and M2-skewed RAW 264.7 cells using mirVana miRNA Isolation Kit (Life Technologies). RNA (2 μg) was converted into cDNA using the High Capacity RNA-to-cDNA Kit (Life Technologies), according to the manufacturer's instructions. The TaqMan Gene Expression Assay for murine *arg1* (Mm00475988_m1), *nos2* (Mm00440502_m1), and *gapdh* (Mm99999915_g1) were purchased from Life Technologies. Quantitative polymerase chain reaction (PCR) analysis was performed using the Applied Biosystems 7500 Fast Real-Time PCR machine. Relative mRNA levels were quantified using the comparative cycle threshold (C_t) method and the formula 2^{-C_t}, with *gapdh* expression as the reference.

Flow Cytometry

Cells were washed with phosphate-buffered saline and incubated with rat anti-mouse FCγIII/II receptor (CD16/CD32; clone 2.4G2; BD Pharmingen, San Jose, California) antibody followed by APC anti-mouse CD115/cFMS/CSF-1R antibody or matched IgG control (Biolegend, San Diego, California). Before acquisition, cells were stained with propidium iodide for gating of live cells. Analysis was performed on 100,000 events collected per sample on Gallios (Beckman Coulter, Brea, California) flow cytometer and analyzed using FlowJo (Tree Star, Ashland, Oregon).

MAFIA Transgenic Mice

MAFIA transgenic mice (C57BL/6-Tg(Csf1r-EGFP-NGFR/FKBP1A/TNFRSF6)2Bck/J) were purchased from The Jackson Laboratory, Bar Harbor, Maine. Offspring were screened by PCR on tail-snip DNA taken at weaning using the Kapa Biosystems mouse genotyping kit, as per the manufacturer's instructions. GFP primers used for the analysis were 5′-AAGTTCATCTGCACCACCG-3′ (forward) and 5′-TCCTTGAAGAAGATGGTGCG-3′ (reverse). PCR thermal conditions were set up according to the protocol provided by The Jackson Laboratory.

Animal Studies

GL261 glioma cells (2×10^4) were implanted (day 0 of the experiment) in the right caudate nucleus of MAFIA mice using a cannulated guide screw system as previously described [20], which had been placed 14 days before. The B/B homodimerizer AP20187 was purchased from Clontech Laboratories, Mountain View, California. Lyophilized AP20187 was dissolved in 100% ethanol at a concentration of 62.5 mg/ml and stored at −20°C. For *in vivo* experiments, treatment solutions were freshly prepared from a dilution of 1.25 mg/ml (as recommended by Clontech Laboratories) consisting of 4% ethanol, 10% PEG-400 (Sigma), and 2% Tween-20 (Fisher Scientific, Pittsburgh, Pennsylvania) in water. The volume of solution was adjusted according to mouse body weight to deliver 5 mg/kg per mouse. AP20187 was injected intraperitoneally daily for 5 days, starting from either the first or the sixth day after glioma implantation. Control animals were treated with vehicle solution alone. Animals were sacrificed when indicated or when exhibiting generalized or local symptoms of disease. Brains were removed, photographed using a digital camera Nikon D60, fixed in 4% formaldehyde for 24 hours at room temperature, and embedded in paraffin. All animal studies were performed in the veterinary facilities

of The University of Texas MD Anderson Cancer Center (Houston, TX) in accordance with institutional guidelines. The largest (*a*) and the smallest (*b*) diameters of the tumors were measured, and tumor volume was calculated using the formula: $a \times b^2 \times 0.4$ [21].

Immunohistochemical and Immunofluorescence Analyses

Paraffin-embedded 5-μm-thick tissue sections were deparaffinized and subjected to graded rehydration before staining. For double immunofluorescence studies [Arginase 1 (Arg1)/GFP, inducible nitric oxide (iNOS)/GFP, Iba1/GFP, CSF-1R/GFP], tissue sections were subjected to heat-induced epitope retrieval (10 mM citrate buffer, pH 6.0) and blocked with 10% serum. Endogenous biotin and streptavidin were blocked using Vector avidin/biotin and streptavidin/biotin kits according to the manufacturer's instructions. Overnight incubation at 4°C with antibodies against Arg1 V-20 (sc-18354; 1:1000; Santa Cruz Biotechnology, Dallas, Texas), iNOS (ab15323; 1:1000; Abcam, Cambridge, Massachusetts), Iba1 (MABN92; 1:1000; Millipore, Billerica, Massachusetts), or CD31 antibody (AF3628, diluted 1:200, R&D Systems) was performed. Bound antibodies were detected by incubation with biotin-conjugated secondary antibody and DyLight 549 or DyLight 488 streptavidin (1:1000; Vector Laboratories, Burlingame, California). Second primary antibodies [GFP (NB600-308; 1:500; Novus Biologicals, Littleton, Colorado), GFP I-16 (sc-5385; 1:100; Santa Cruz Biotechnology), and CSF-1R/cFMS (sc-692; 1:200; Santa Cruz Biotechnology)] were incubated overnight at 4°C and developed with Alexa Fluor 488– or Alexa Fluor 594–conjugated secondary antibodies (1:1000; Invitrogen, Grand Island, New York). Fluorescence-labeled slides were counterstained with 4′,6-diamidino-2-phenylindole (DAPI; Sigma), mounted with fluorescence mounting medium (Dako, Carpinteria, California), and examined under a Zeiss Axiovert 200 M fluorescence microscope or a confocal microscope (Olympus Fluoview FV1000).

For Ki67 immunohistochemical analysis, endogenous peroxidase activity was quenched with 0.3% H_2O_2. Sections were blocked with 10% horse serum and a Vector avidin/biotin kit. Incubation with Ki67 MM1 antibody (VP-K452; 1:100; Vector Laboratories) was performed overnight at 4°C. Sections were then incubated with biotinylated secondary antibody followed by peroxidase-conjugated streptavidin (1:500; Beckman Coulter). The reaction was developed using stable 3,3′-diaminobenzidine (DAB, Research Genetics, Huntsville, Alabama). After immunoreaction, sections were counterstained with Harris hematoxylin and mounted with Cytoseal 60 (Thermo Scientific, Waltham, Massachusetts). Images were captured using a bright-field microscope (Zeiss Axioskop 40).

For immunofluorescence and immunohistochemical analysis, 10 pictures were acquired randomly from central or peripheral areas of tumors and, when indicated, from contralateral cerebral hemispheres under ×20 or ×40 objectives. A minimum of three animals from each experimental group was analyzed. The number of GFP^+, $Ki67^+$, $Arg1^+/GFP^+$, and $iNOS^+/GFP^+$ cells was quantified in a double-blind manner by two different researchers.

Quantification of Microvessel Density

Areas containing the most microvessels (or tumor "hot spots") were identified following immunostaining with anti-CD31 antibody. Sections were examined with a fluorescence microscope at low magnification (original magnification, ×40 and ×100), as previously described [22]. Then, the individually stained microvessels in these areas were counted at ×200 magnification over a square grid that corresponded to a field size of 0.16 mm^2. Large microvessels and single endothelial cells that were clearly separate from the microvessels were included in the microvessel count; branching structures were counted as one vessel, unless there was a break in the continuity of the vessel, in which case it was counted as two distinct vessels. The mean number of microvessels counted in five fields was used for analyses.

Statistical Analysis

Data are presented as mean ± SD. The *P* value for difference between samples was calculated using double-sided Student's *t* test. $P < .05$ was considered statistically significant.

Results

Kinetics of GL261 Glioma Intracranial Growth and Tumor-Associated Microglia/Macrophage Population in MAFIA Transgenic Mice

To determine the kinetics of GL261 glioma growth in MAFIA transgenic mice, we first analyzed tumor morphologic characteristics on days 5, 10, 14, and 19 after tumor cell implantation (Figure 1*A*). We performed hematoxylin and eosin (H&E) and Ki67 staining to assist in the analysis of tumor morphology and tumor growth (Figure 1*B*). On days 5 and 10 after tumor cell inoculation, GL261-derived tumors exhibited multifocal distribution of $Ki67^+$ cells in the area of injection of the brain parenchyma. On day 14, the tumors were clearly established and highly proliferative, with exponential growth. By day 19, the tumor occupied almost the entire left hemisphere with slightly less cell density that was due probably to the presence of dilated vascular structures. At that time point, examination of the brain itself revealed secondary effects to tumor mass pressure, such as midline shift and ventricular compression. The tumor/normal brain edge was well defined, and no significant signs of invasiveness were observed.

To identify the presence of tumor-associated microglia/macrophages in MAFIA mice, we performed GFP immunofluorescence staining. As early as 5 days after GL261 implantation, compared to the presence of GFP^+ cells in contralateral, non-tumor containing hemispheres, the presence of GFP^+ cells had increased (Figure 2*A*), which was suggestive of activation/infiltration of myeloid cells into the tumor. Thus, in tumor-free hemispheres, we detected relatively few microglia in the resting stage, with thin branching processes, and small cell bodies (Figure 2*A*). GL261-derived tumors analyzed 10 days after cell implantation displayed microglia/macrophages with morphology compatible with activation as demonstrated by their augmented cell body size and amoeboid morphology. The density of GFP^+ cells within the tumor continued to increase, and by day 14 post-implantation, the tumors harbored an even greater number of glioma-infiltrating microglia/macrophages. Interestingly, the density of these GFP^+ cells decreased significantly from day 14 to day 19 ($P < .001$), associated to a decreased cellularity due to the presence of necrotic areas as previously reported [23], whereas the number of GFP^+ cells (i.e., microglia/macrophages) at the tumor periphery increased ($P < .05$; Figure 2, *B* and *C*). In sham-operated animals analyzed 5 and 10 days after mock implantation (Figure W1*A*), we did not observe accumulation of GFP^+ cells in the injection area, indicating that the recruitment or activation of microglia/macrophages into the tumor was initiated by the presence of glioma cells (Figure W1*B*).

To characterize the GFP^+ population in the MAFIA model, we analyzed the expression of Iba1 (which is highly expressed in cells of the monocyte/macrophage lineage), and CSF-1R, by double immunofluorescence. As expected, GFP and CSF-1R expression

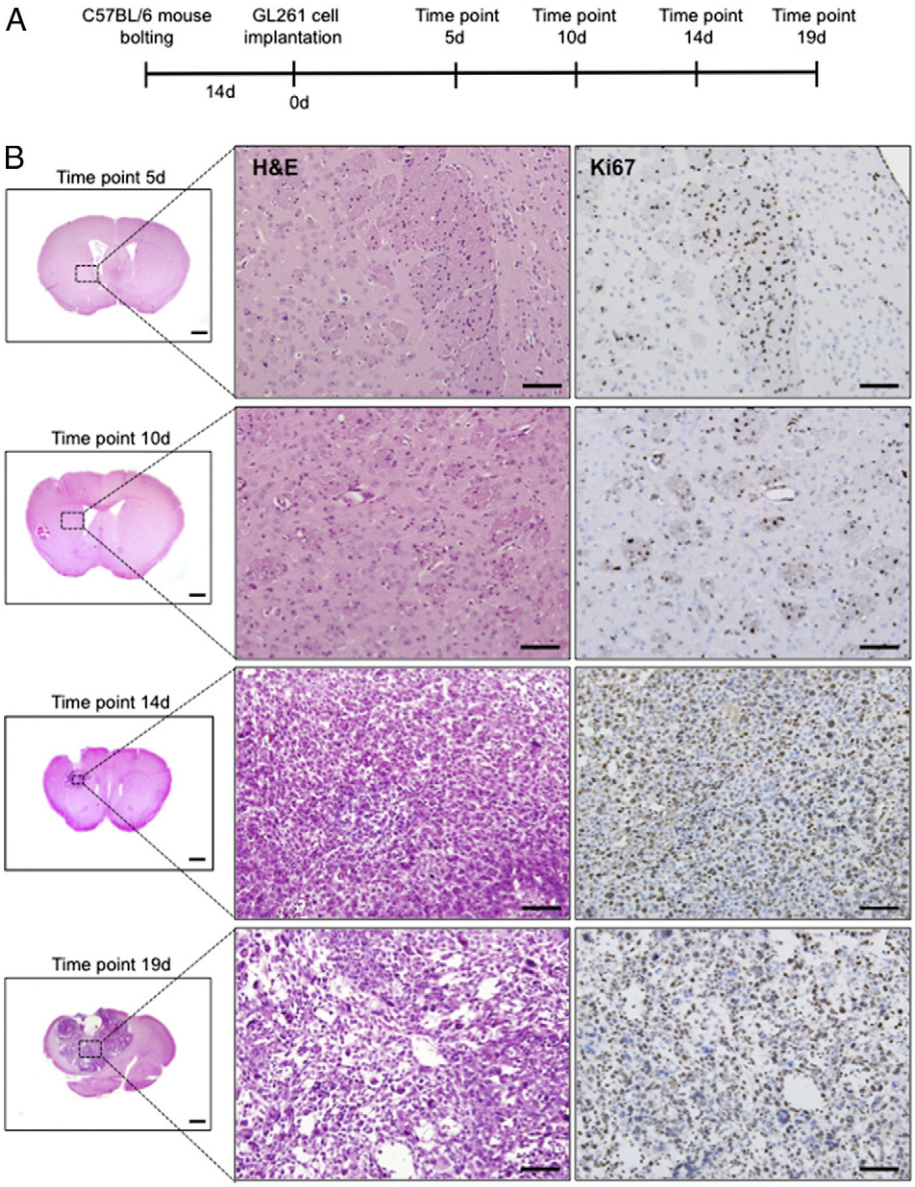

Figure 1. Kinetics of GL261 intracranial glioma growth in MAFIA transgenic mice. (A) Scheme of the experiment. Briefly, MAFIA mice underwent guided screw cannulation, and 14 days later, GL261 cells were implanted into the right caudate nucleus. Animals were sacrificed 5, 10, 14, or 19 days after cell implantation, and their brains were assessed for morphologic characteristics. (B) Representative images of H&E (left and middle columns) and Ki67 (right column) staining of GL261 intracranial glioma sections from mice sacrificed at the indicated time points after tumor cell implantation. Scale bar, 500 μm (whole-brain tissue) or 50 μm (insets).

was co-localized in tumor and intact brain (Figure W2*A*). Our data show that, within the tumoral area, most Iba1$^+$ cells (microglial) are GFP$^+$ (82.1 ± 1.46%). Of note, in normal brain, all Iba1$^+$ cells were GFP$^+$ (Figure W2*B*). These data indicate that CSF-1R–expressing cells encompass an important population, although not all monocyte/macrophage lineage cells present in the glioma-bearing brain were Iba1$^+$, as previously found in other organs of this transgenic model using F4/80 as a macrophage marker [10].

To further characterize the phenotype of the tumor-associated microglia/macrophages, we analyze the expression of Arg1 (an M2 phenotype marker) and iNOS (an M1 phenotype marker) [24–26]. To this end, we performed double immunofluorescence staining for GFP/Arg1 and GFP/iNOS expression in sections of brains of GL261-bearing mice sacrificed at different times after cell implantation. No Arg1$^+$ cells were detected at day 5, but we observed the presence of double-positive (GFP$^+$/Arg1$^+$) cells at day 10, which exhibited a more rounded morphology and cellular processes compatible with early stages of microglia activation. Quantification of the Arg1$^+$/GFP$^+$ cells at 14 and 19 days after GL261cell implantation showed that 98 ± 1.5% of Arg1$^+$ cells expressed the GFP antigen, suggesting that Arg1 is expressed by microglia/macrophages, and those exhibited an amoeboid morphology suggestive of an activate cellular stage. In addition, we observed that 50% to 75% of GFP$^+$ cells expressed Arg1 and that the number of M2-polarized microglia/macrophages at the tumor-normal brain edge tended to increase during glioma growth (Figure 3, *A* and *B*). In contrast, we did not detect iNOS$^+$ cells in early stages of glioma growth (days 5 and 10; Figure 3*C*) or in tumor-normal edges at later

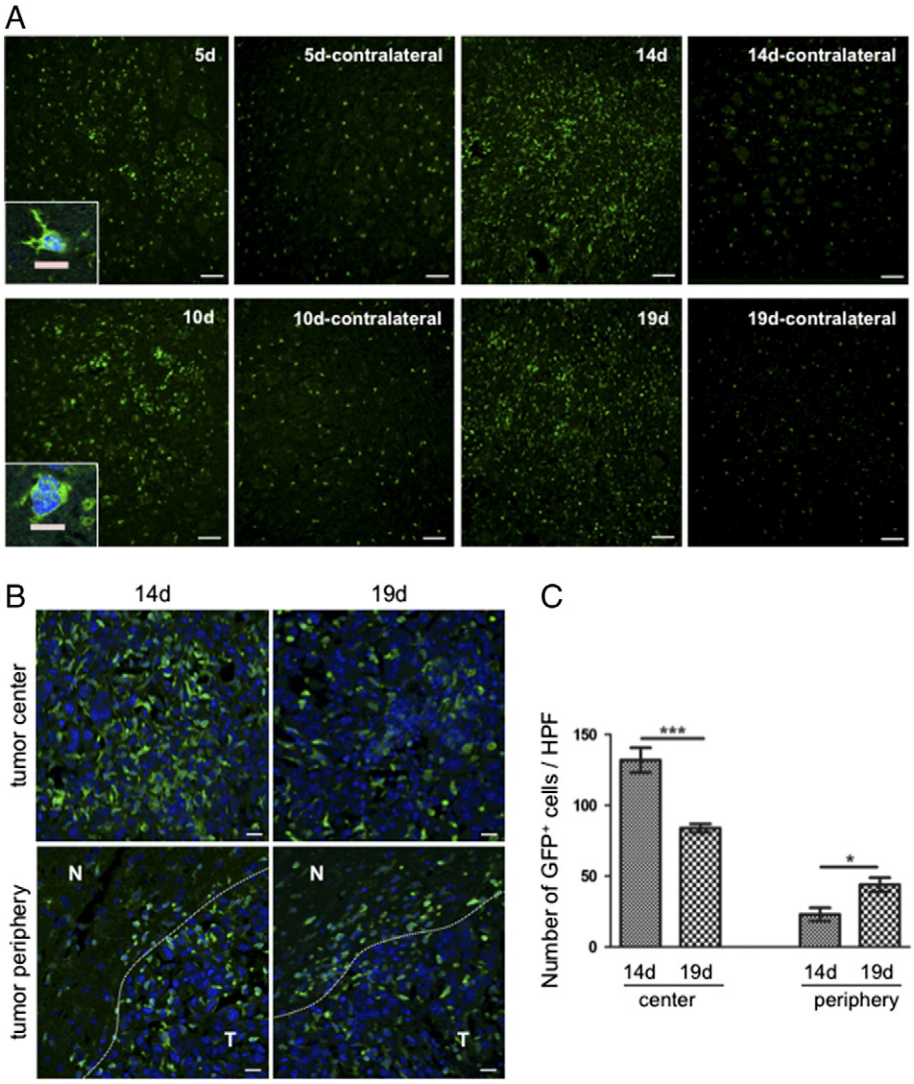

Figure 2. Microglia/macrophage accumulation in tumor-bearing hemisphere. (A) Representative images of GFP staining using fluorescent microscopy show the presence of microglia/macrophages in tumor-bearing hemispheres, analyzed at the indicated time points after GL261 cell implantation. Images of contralateral, non–tumor-bearing hemispheres are shown for comparison. Scale bar, 100 μm. Insets show detailed cellular morphology. Scale bar, 60 μm. (B) Representative confocal microscopy images of GFP staining from the center and periphery of tumors. Dashed line, approximate tumor (T)/normal brain (N) edge. Scale bar, 20 μm. (C) Quantification of GFP$^+$ cells ($\times$400) present in the tumor area and in the tumor-normal brain edge area (periphery) on sections of brains from animals sacrificed on day 14 or 19 post-implantation. HPF, high-powered field. Data are presented as mean ± SD (n = 3 mice). *** $P < .001$ and * $P < .05$.

stages of tumor development. In fact, we identified very few iNOS$^+$ cells expressing GFP in central tumor areas at late stages of tumor development (days 14 and 19; Figure 3*C*). These findings suggest that M2-polarized glioma-associated macrophages constitute the predominant population in GL261-derived intracranial gliomas. Of interest, most of the Arg1$^+$ cells expressed GFP and approximately 70% of iNOS-positive cells in the whole tumor area expressed the fluorescent protein (72 ± 12.8%). These data suggest that M2-polarized macrophages constitute the major CSF-1R$^+$ population, in agreement with our *in vitro* polarization studies (Figure W3) and a recent report that examined human macrophages [27].

Ablation of Macrophages in the MAFIA Model Impairs Inflow of Myeloid Cells into the Tumor and Promotes Skew Toward the M1 Phenotype

To understand the role of microglia/macrophages in glioma development, we targeted this population by administering for five consecutive days (1-5 days or 6-10 days) after cell implantation the B/B homodimerizer drug AP20187 to mice bearing GL261 intracranial tumors (Figure W4*A*). As mentioned previously, AP20187 induces Fas-mediated apoptosis through activation of the caspase-8 pathway in myeloid lineage cells. The day after treatment was completed (day 6 for group A and day 11 for group B), brains were analyzed for GFP$^+$ cells. In tumor-containing hemispheres, the GFP$^+$ cells were forcefully depleted (Figure W4*B*). The presence of GFP$^+$ cells in the contralateral, non–tumor-containing hemisphere was not affected by the treatment (data not shown). Our data suggested that normal microglia is not targeted by AP20187, which is consistent with previous reports showing the inability of this drug dimerization to cross the blood-brain barrier [10,28].

To analyze the long-term impact of pharmacological targeting of the macrophage/microglia population in glioma tumors, we allowed for full glioma development in both group A and group B of the experiment (Figure 4*A*). Control animals were sacrificed between 16

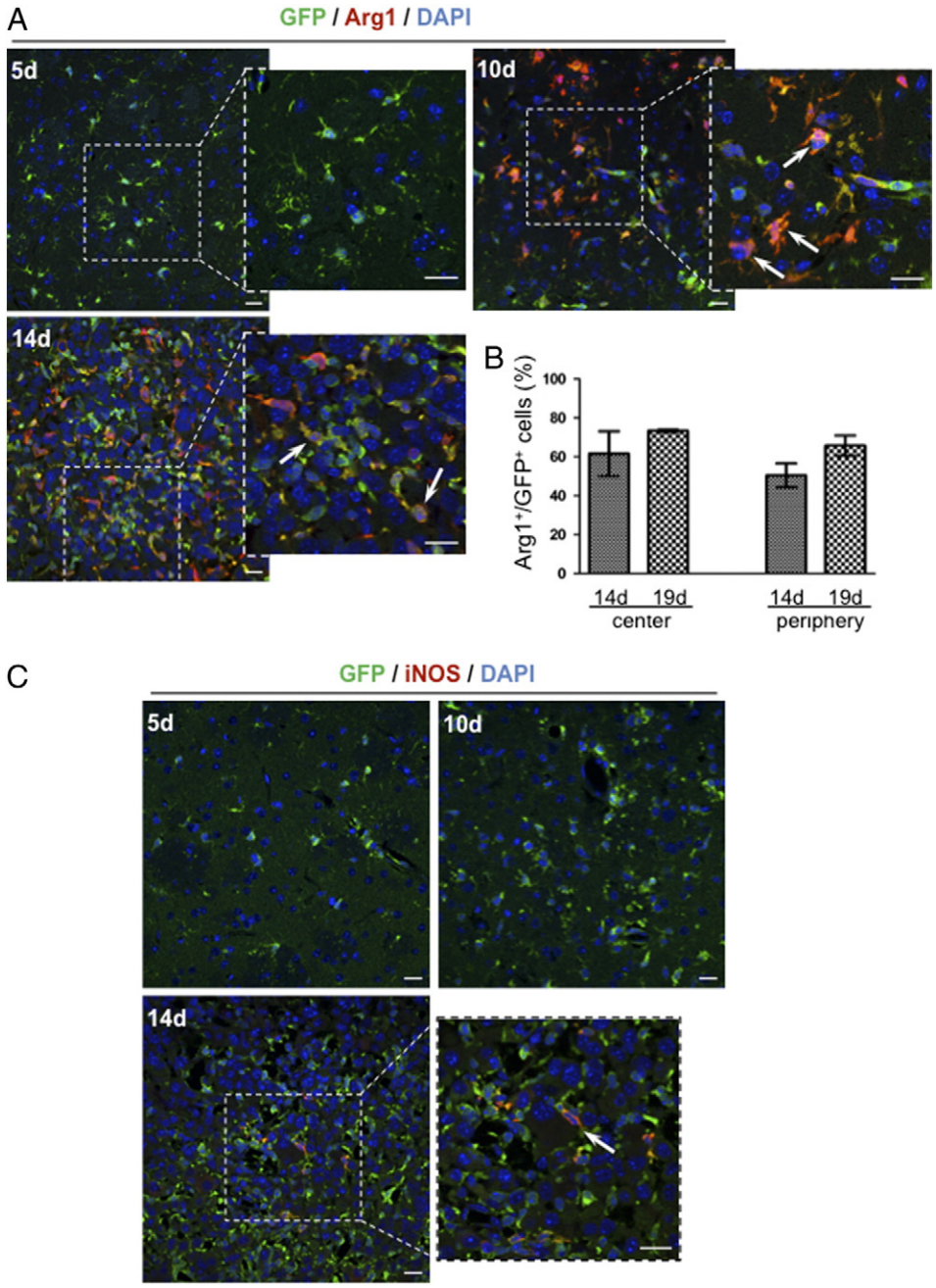

Figure 3. Phenotypic characterization of the glioma-associated microglia/macrophage population. (A) Representative confocal images of Arg1 (red) and GFP (green) staining in brain sections from GL261 glioma–bearing animals sacrificed on day 5, 10, or 14 post-implantation. (Inset) White arrows highlight the increase in the number of $Arg1^+/GFP^+$ cells and change in morphology over time. DAPI (blue) was used for cellular nuclear staining. Scale bar, 20 μm. (B) Quantification of $Arg1^+/GFP^+$ cells in the center and periphery of tumors from mice sacrificed on day 14 or 19. Data are presented as mean ± SD (n = 3 mice). (C) Representative confocal images of iNOS (red) and GFP (green fluorescence) staining of brains of tumor-bearing mice sacrificed at the indicated times. (Inset) White arrows highlight the rare $iNOS^+/GFP^+$ cells, which were observed only at day 14. DAPI (blue) was used for nuclear staining. Scale bar, 20 μm.

and 20 days after cell implantation, when signs of disease burden were evident. Although AP20187-treated animals did not show signs compatible with glioma progression, we decided, on this time period, to have a more accurate comparison of tumor growth and analysis of the macrophage population. Analysis of the brains of the AP20187-treated animals revealed fewer GFP^+ cells within tumors. We found that early ablation of macrophage cells (1-5 days post-implantation) resulted in an approximately 50% reduction in the number of GFP^+ cells in tumors ($P < .01$ *vs* control), while postponed treatment (6-10 days post-implantation) diminished the accumulation of GFP^+ cells in tumors by 65% ($P < .001$ *vs* control; Figure 4, *B* and *C*). Moreover, we found significantly fewer microglia/macrophages infiltrating the tumor periphery (by ~60%) in both early and postponed myeloid cell ablation (control *vs*

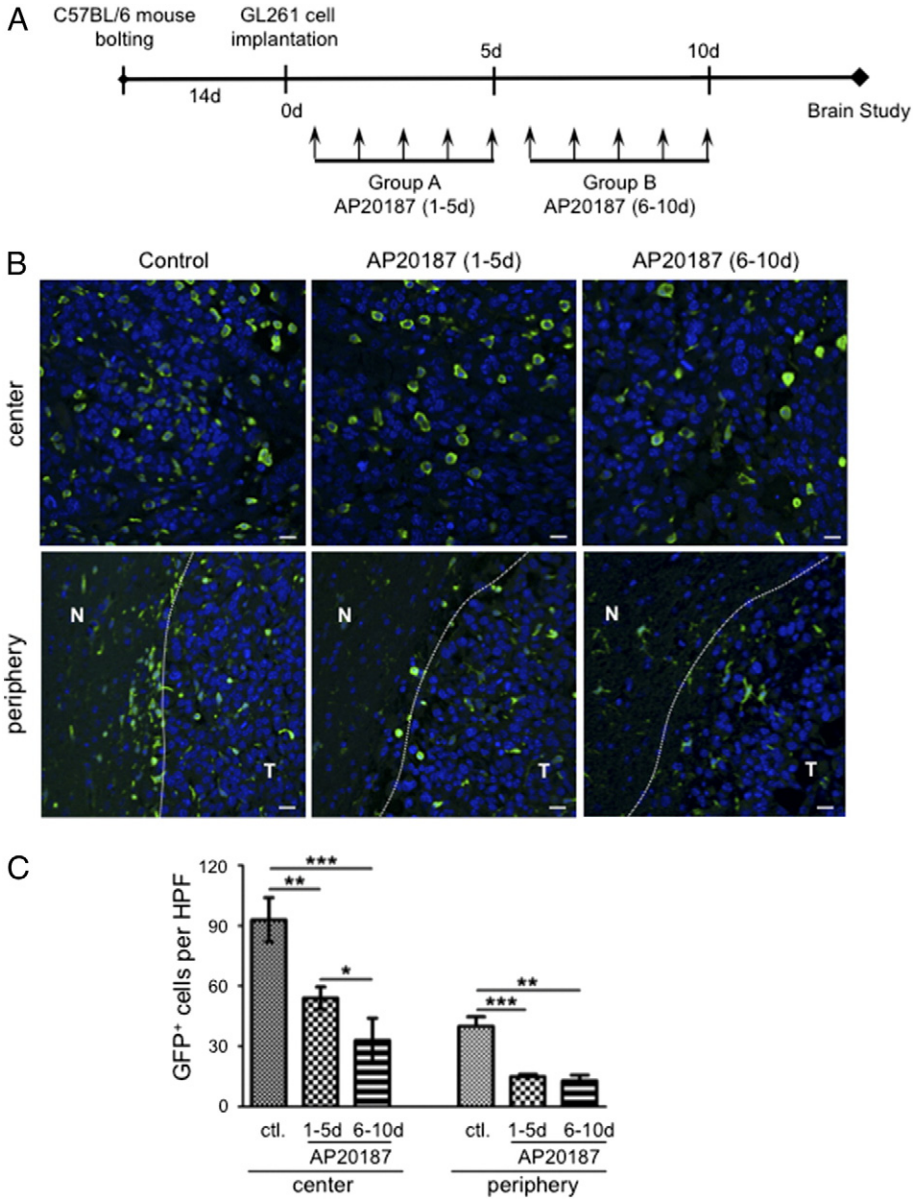

Figure 4. Influence of conditional macrophage ablation on tumor-associated myeloid cell reconstitution. (A) Scheme of the experiment. Briefly, GL261 cells were implanted into the right caudate nucleus of MAFIA mice. AP20187 or vehicle was administered daily from days 1 to 5 (group A) or from days 6 to 10 (group B) of the experiment. Animals were sacrificed 16 to 21 days after cell implantation. (B) Tumor sections from vehicle- or AP20187-treated mice were stained for GFP expression. Representative images from the center (upper row) and periphery (lower row) of tumors were acquired using confocal microscopy. Dashed line, approximate tumor (T)/normal brain tissue (N) edge. DAPI was used as nuclear staining. Scale bar, 20 μm. (C) Number of GFP$^+$ cells per HPF ($\times$ 400). Data are presented as mean $\pm$ SD (n = 3 mice). *** $P < .001$, ** $P < .01$, and * $P < .05$.

AP20187 on days 1-5, $P < .001$; control *vs* AP20187 on days 6-10, $P < .01$). Ablation had no notable effect on microglia in intact brain, including the contralateral hemisphere.

To determine the impact of the temporal ablation of microglia/macrophages on the reconstitution of the tumor-associated myeloid population phenotype, we used double immunofluorescence to analyze the M1 and M2 status of those cells. Confocal analysis of Arg1$^+$ and GFP$^+$ cells in control mice showed that both early (1-5 days) and postponed (6-10 days) injection of the dimerization agent AP20187 reduced the number of double positive, Arg1$^+$GFP$^+$ cells in the center and periphery of the tumor ($P < .01$ and $P < .001$, respectively; Figure 5*A*). These results suggested that the number of M2-like polarized cells in the reconstituted pool decreased.

We then analyzed the M1 polarization of the reconstituted pool by performing double immunofluorescence image for GFP and iNOS. As we expected, iNOS$^+$ cells within the tumor of control-treated MAFIA mice were rarely detected and appeared to be randomly distributed. Interestingly, agglomerations of iNOS$^+$GFP$^+$ cells were observed in tumor central areas in mice in which myeloid cell ablation was performed (Figure 5*B*). Compared with mice treated with AP20187 on days 1 to 5 and days 6 to 10, the number of iNOS$^+$GFP$^+$ cells in control-treated mice was approximately seven-fold and two-fold higher, respectively.

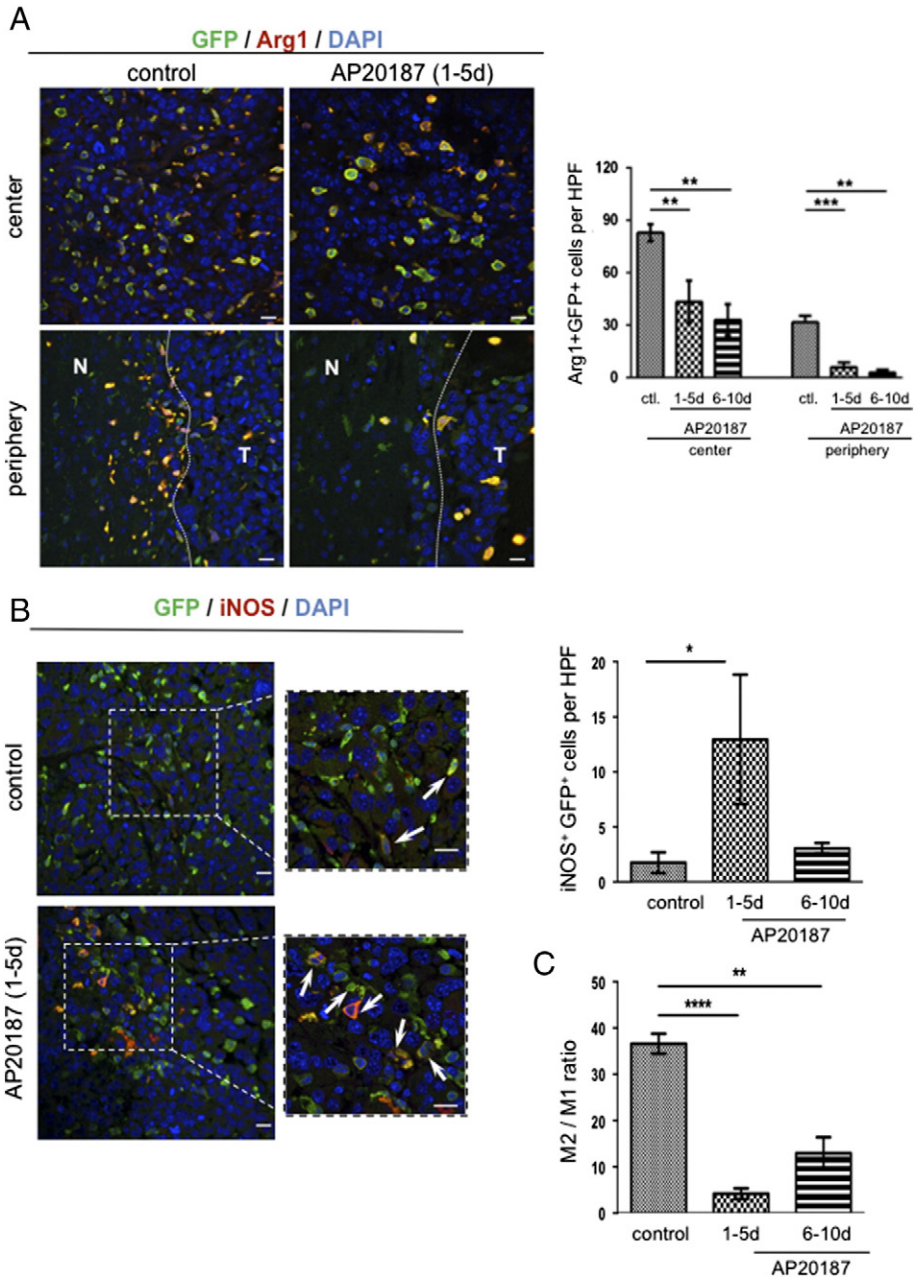

Figure 5. Modifications in the repopulation of M1/M2-polarized myeloid cells after macrophage ablation. (A) Representative images of double immunofluorescence analysis for the expression of Arg1 (red) and GFP (green) in GL261-derived tumors of vehicle- or AP20187-treated MAFIA mice. DAPI (blue) was used for nuclear staining. Curved dashed lines indicate the approximate tumor (T)/normal brain (N) edge. Scale bar, 20 μm. The graph shows the number of double positive Arg1$^+$GFP$^+$ cells per HPF ($\times$400; central and peripheral areas). Data are presented as mean ± SD (n = 3 mice). (B) Representative images of sections from tumor-bearing mice treated with vehicle solution or AP20187 that were stained for iNOS and GFP expression. (Insets) Arrows point to iNOS$^+$GFP$^+$ cells. Scale bar, 20 μm. Quantitative analysis of the number of double positive iNOS$^+$GFP$^+$ cells per HPF in GL261-derived intracranial tumors from control or AP20187-treated mice (central areas). Data are presented as mean ± SD (n = 3 mice). (C) Quantitative analysis of M1 ratio as the/M1 ratio as the number of double positive Arg1$^+$GFP$^+$ cells per HPF *versus* the number of double positive iNOS$^+$GFP$^+$ cells per HPF in GL261-derived intracranial tumors from control or AP20187-treated mice (central areas). **** $P < .0001$, *** $P < .001$, ** $P < .01$, and * $P < 0.05$.

The data obtained suggested an M2-to-M1 shift in the phenotype of the reconstituted myeloid population present in the glioma microenvironment of MAFIA mice. Specifically, the M2/M1 ratio on reconstitution decreased by nine-fold and three-fold in mice treated with AP20187 on days 1 to 5 and days 6 to 10, respectively (Figure 5*C*; $P < .0001$ and $P < .01$, respectively).

Taken together, our results suggested that ablation of the CSF-1R$^+$ myeloid population substantially alters the relative M1 and M2

representation in the tumor microenvironment and, subsequently, the functionality of the macrophage/microglia population.

Myeloid Cell Ablation Strongly Impairs the Growth of Intracranial Glioma

To further explore the effect of temporal ablation of the tumor-infiltrating myeloid cells (CSF-1R–GFP$^+$ cells) on glioma growth, we analyzed the phenotype of the tumors of MAFIA mice treated with AP20187 and compared it with tumors in control-treated mice (Figure 4*A*). Tumor volume analysis revealed that microglia/macrophage-depleted mice had smaller tumors, approximately 50% in size, than those of vehicle-treated animals (Figure 6, *A–C*, control *vs* AP20187 on days 1-5d and on days 6-10; $P < .05$ for both comparisons), suggesting that microglia/macrophage ablation resulted in decreased tumor growth.

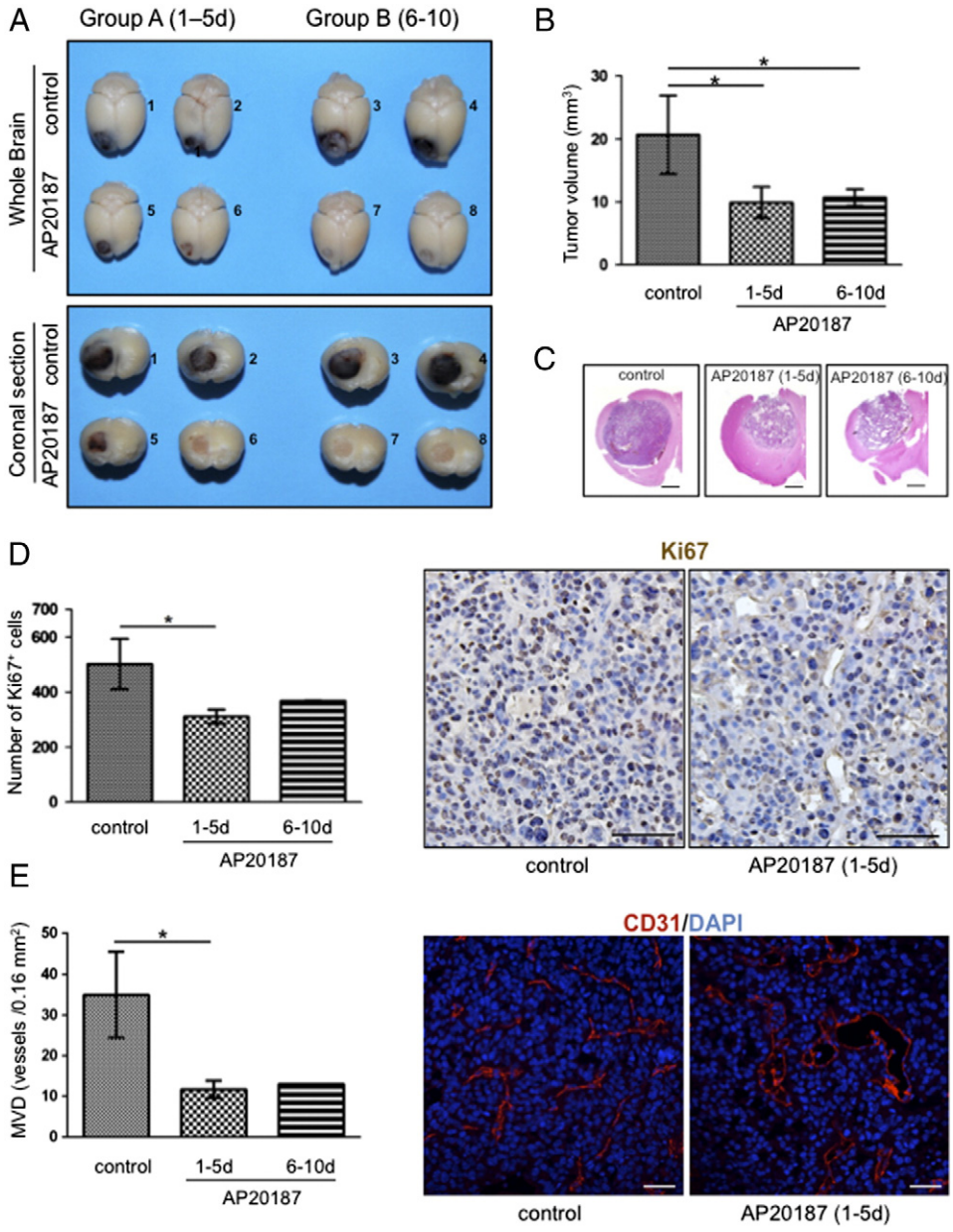

Figure 6. Outcome of temporal macrophage ablation on tumor growth. Design of experiment is described in Figure 4*A*. (A) Macroscopic photos of whole brains and coronal sections. Numbers (1-8) represent individual tumor-bearing mice. (B) Tumor volume in control-treated and AP20187-treated mice ($n = 6$ mice in control-treated group and $n = 3$ mice in each AP20187-treated group). Data are presented as mean ± SD. * $P < .05$. (C) Representative H&E-stained sections from each experimental group. Scale bar, 500 μm. (D) Number of Ki67$^+$ cells in tumors from control-treated and AP20187-treated MAFIA mice. (Left panel) Data are presented as mean ± SD of Ki67$^+$ cells scored from three or four microscopic fields (× 200). * $P < .05$. (Right panel) Representative microscopic pictures showing distribution of Ki67$^+$ cells (brown; nuclear staining) in both control- and AP20187 (days 1-5)-treated animals. Scale bar, 50 μm. (E) Quantification of microvessel density in tumors from control-treated and AP20187-treated MAFIA mice. (Left panel) Data are presented as mean ± SD of microvessel density scored from three or four microscopic fields (× 200). * $P < .05$. (Right panel) Representative microscopic pictures showing vascular structures (CD31$^+$, red fluorescence) in both control- and AP20187 (days 1-5)-treated animals. DAPI (blue) was used for nuclear staining. Scale bar, 50 μm.

To further evaluate the impact of the decrease in microglia/macrophage cells on tumor proliferation, we measured the number of Ki67$^+$ cells within tumors. This analysis revealed a decrease of approximately 50% in the mitotic index when AP20187 was started immediately after tumor implantation (days 1-5, $P < .05$) or after 6 days ($P = .0562$; Figure 6*D*). Of note, AP20187 treatment (ranging 0.01 to 10 nM) did not affect GL261 glioma cells or genetically wild-type RAW 264.7 macrophages as assessed by an *in vitro* viability assay (data not shown), suggesting that the treatment did not affect unexpected target populations. In addition, temporary ablation of CSF-1R–GFP$^+$ cells resulted in decreased microvascular density after both AP20187 treatment regimens ($P < .05$; Figure 6*E*). Together, our results showed that temporal ablation of myeloid populations resulted in decrease of the tumor proliferative and angiogenic properties, affecting significantly tumor growth.

Discussion

Here, we report that conditional and temporal ablation of the CSF-1R$^+$ population affect the reconstituted glioma myeloid population. Specifically, such ablation results in an increased M1/M2 ratio that, in turn, was associated with decreased tumor mitotic index, angiogenesis, and growth. Furthermore, we validated the use of the MAFIA transgenic model for further preclinical studies of brain tumors.

We found that the kinetics of the GL261 intracranial glioma growth in this transgenic model were similar to those previously described for other models [29–31]. Of interest, we observed an initial adaptive phase characterized by small islets of tumor cells scattered around the injection site, with exponential tumor growth after day 10 after tumor cell implantation. Consistent with other studies [22,27,32], GL261 intracranial glioma was characterized by tumoral microglia/macrophage infiltration, which was easily identified in the MAFIA model as accumulation of easily GFP-trackable cells. Our study also provided evidence of an increased presence of a microglia/macrophage population, which underwent morphologic modifications in the tumoral area during the adaptive tumoral phase, suggestive of a shift from a resting to an active state.

To further study the tumor infiltrating microglia/macrophage population, we performed immunofluorescence analysis to discriminate between the classically activated M1 and the alternatively activated M2 microglia/macrophage phenotype [3,33,34]. Although glioma-infiltrating GFP$^+$ microglia/macrophages were evident within 5 days after cell implantation, they did not express detectable levels of the M2 marker Arg1 [24–26] until late in the adaptation stage. Furthermore, the accumulation of Arg1$^+$ cells increased over time to represent the largest GFP$^+$ microglia/macrophage population within 14 days after cell implantation. However, GFP$^+$ cells rarely colocalized with the M1 marker iNOS [24–26], which confirmed a predominant M2 phenotype or protumorigenic phenotype of the microglia/macrophages associated with the GL261 glioma model [32].

Our data showed that conditional temporal ablation of microglia/macrophages was successfully achieved using the MAFIA transgenic model. Other pharmacological ablation methodologies, such as clodronate liposomes, are less selective in that they deplete cells depending on their phagocytic properties, including subtypes of T cells, and might fail to target other cells of peripheral macrophage lineage that eventually would be recruited as TAMs [10,14,28]. Of note, in the MAFIA transgenic model, ablation of normal CSF-1R$^+$ microglia in the contralateral, non–tumor-bearing hemisphere was not noted, probably because of the inability of the dimerization treatment to cross the intact blood-brain barrier [10,14,23,28].

Interestingly, we found that conditional ablation, although transient, significantly affected the number and phenotype of the reconstituted pool of tumor-associated myeloid cells, which reduced the presence of GFP$^+$ cells in tumors by 40% to 80%. Furthermore, the infiltrating population switched the polarization status due to a decrease in the M2 population. The presence of M2-polarized microglia/macrophages positively correlates with malignancy in gliomas; therefore, modifying the landscape scenario toward a more M1-like phenotype may be a useful strategy for glioblastoma therapy. Our results are in line with other efforts to neutralize tumor-associated chronic inflammation, such as blocking the nuclear factor kappa-light-chain-enhancer of activated B cells (NFκB) or signal transducer and activator of transcription 3/6 (STAT3/6) pathway or inhibiting cytokine pathways that dictate the recruitment or immune cell function, such as CSF-1 or chemokine (C-C motif) ligand 2 (CCL2) [34,35].

The work presented here demonstrated that temporal ablation of the macrophage population is sufficient to achieve a significant anti-glioma effect. The role of M2-polarized macrophages in promoting angiogenesis, cell migration and invasion, and an immunosuppressive tumor environment might explain that the decrease in number of GFP$^+$ cells and M2/M1 ratio in the reconstituted population resulted in a decrease in tumor growth, angiogenesis, and proliferation in the model here studied [3]. Importantly, the MAFIA transgenic model is designed to both detect and target cells that express CSF-1R. This offers an interesting parallelism with recent studies that showed the CSF-1R inhibitor, BLZ945, resulted in both decreased M2 macrophage markers and subsequent tumor growth in a proneural glioma model [36]. Similarly, studies in other types of cancers using a monoclonal antibody that inhibits CSF-1R activation, RG7155, resulted in preferential targeting of the M2-polarized populations [27] and a subsequent increase in CD8$^+$ T cell population [35] and decrease in FoxP3$^+$ T regulatory cells [27].

In conclusion, we demonstrated that temporal ablation of macrophages in the MAFIA model results in an M2-to-M1 shift in the reconstituted myeloid population, which decreased tumor proliferation, angiogenesis, and growth. In addition, the intracranial glioma MAFIA transgenic model is an interesting tool for examining the putative role of macrophages in therapy resistance and for modeling the effect of new drugs targeting macrophages, either as single agents or in combination with glioma-targeted therapies.

Supplementary data to this article can be found online at http://dx.doi.org/10.1016/j.neo.2015.03.003.

Acknowledgements

We thank Elizabeth L. Hess (Department of Scientific Publications, The University of Texas MD Anderson Cancer Center) and Brittany C. Parker (Department of Neurosurgery, The University of Texas MD Anderson Cancer Center) for editing. We thank Verlene Henry for animal technical support (Brain Tumor Program, The University of Texas MD Anderson Cancer Center).

References

[1] Hanahan D and Weinberg RA (2011). Hallmarks of cancer: the next generation. *Cell* **144**, 646–674.

[2] Charles NA, Holland EC, Gilbertson R, Glass R, and Kettenmann H (2012). The brain tumor microenvironment. *Glia* **60**, 502–514.

[3] Qian BZ and Pollard JW (2010). Macrophage diversity enhances tumor progression and metastasis. *Cell* **141**, 39–51.

[4] Bingle L, Brown NJ, and Lewis CE (2002). The role of tumour-associated macrophages in tumour progression: implications for new anticancer therapies. *J Pathol* **196**, 254–265.

[5] Heusinkveld M and van der Burg SH (2011). Identification and manipulation of tumor associated macrophages in human cancers. *J Transl Med* **9**, 216.

[6] Nishie A, Ono M, Shono T, Fukushi J, Otsubo M, Onoue H, Ito Y, Inamura T, Ikezaki K, and Fukui M, et al (1999). Macrophage infiltration and heme oxygenase-1 expression correlate with angiogenesis in human gliomas. *Clin Cancer Res* **5**, 1107–1113.

[7] Rossi ML, Jones NR, Candy E, Nicoll JA, Compton JS, Hughes JT, Esiri MM, Moss TH, Cruz-Sanchez FF, and Coakham HB (1989). The mononuclear cell infiltrate compared with survival in high-grade astrocytomas. *Acta Neuropathol* **78**, 189–193.

[8] Galarneau H, Villeneuve J, Gowing G, Julien JP, and Vallieres L (2007). Increased glioma growth in mice depleted of macrophages. *Cancer Res* **67**, 8874–8881.

[9] Zhai H, Heppner FL, and Tsirka SE (2011). Microglia/macrophages promote glioma progression. *Glia* **59**, 472–485.

[10] Burnett SH, Kershen EJ, Zhang J, Zeng L, Straley SC, Kaplan AM, and Cohen DA (2004). Conditional macrophage ablation in transgenic mice expressing a Fas-based suicide gene. *J Leukoc Biol* **75**, 612–623.

[11] Winkler IG, Sims NA, Pettit AR, Barbier V, Nowlan B, Helwani F, Poulton IJ, van Rooijen N, Alexander KA, and Raggatt LJ, et al (2010). Bone marrow macrophages maintain hematopoietic stem cell (HSC) niches and their depletion mobilizes HSCs. *Blood* **116**, 4815–4828.

[12] Chang MK, Raggatt LJ, Alexander KA, Kuliwaba JS, Fazzalari NL, Schroder K, Maylin ER, Ripoll VM, Hume DA, and Pettit AR (2008). Osteal tissue macrophages are intercalated throughout human and mouse bone lining tissues and regulate osteoblast function in vitro and in vivo. *J Immunol* **181**, 1232–1244.

[13] Alexander KA, Chang MK, Maylin ER, Kohler T, Muller R, Wu AC, Van Rooijen N, Sweet MJ, Hume DA, and Raggatt LJ, et al (2011). Osteal macrophages promote in vivo intramembranous bone healing in a mouse tibial injury model. *J Bone Miner Res* **26**, 1517–1532.

[14] Steel CD, Kim WK, Sanford LD, Wellman LL, Burnett S, Van Rooijen N, and Ciavarra RP (2010). Distinct macrophage subpopulations regulate viral encephalitis but not viral clearance in the CNS. *J Neuroimmunol* **226**, 81–92.

[15] Sun Y, Karmakar M, Roy S, Ramadan RT, Williams SR, Howell S, Shive CL, Han Y, Stopford CM, and Rietsch A, et al (2010). TLR4 and TLR5 on corneal macrophages regulate *Pseudomonas aeruginosa* keratitis by signaling through MyD88-dependent and -independent pathways. *J Immunol* **185**, 4272–4283.

[16] Sasmono RT, Oceandy D, Pollard JW, Tong W, Pavli P, Wainwright BJ, Ostrowski MC, Himes SR, and Hume DA (2003). A macrophage colony-stimulating factor receptor-green fluorescent protein transgene is expressed throughout the mononuclear phagocyte system of the mouse. *Blood* **101**, 1155–1163.

[17] Cecchini MG, Dominguez MG, Mocci S, Wetterwald A, Felix R, Fleisch H, Chisholm O, Hofstetter W, Pollard JW, and Stanley ER (1994). Role of colony stimulating factor-1 in the establishment and regulation of tissue macrophages during postnatal development of the mouse. *Development* **120**, 1357–1372.

[18] Clifford AB, Elnaggar AM, Robison RA, and O'Neill K (2013). Investigating the role of macrophages in tumor formation using a MaFIA mouse model. *Oncol Rep* **30**, 890–896.

[19] Schwertfeger KL, Xian W, Kaplan AM, Burnett SH, Cohen DA, and Rosen JM (2006). A critical role for the inflammatory response in a mouse model of preneoplastic progression. *Cancer Res* **66**, 5676–5685.

[20] Lal S, Lacroix M, Tofilon P, Fuller GN, Sawaya R, and Lang FF (2000). An implantable guide-screw system for brain tumor studies in small animals. *J Neurosurg* **92**, 326–333.

[21] Attia MA and Weiss DW (1966). Immunology of spontaneous mammary carcinomas in mice. V. Acquired tumor resistance and enhancement in strain A mice infected with mammary tumor virus. *Cancer Res* **26**, 1787–1800.

[22] Lee OH, Fueyo J, Xu J, Yung WK, Lemoine MG, Lang FF, Bekele BN, Zhou X, Alonso MA, and Aldape KD, et al (2006). Sustained angiopoietin-2 expression disrupts vessel formation and inhibits glioma growth. *Neoplasia* **8**, 419–428.

[23] Leten C, Struys T, Dresselaers T, and Himmelreich U (2014). In vivo and ex vivo assessment of the blood brain barrier integrity in different glioblastoma animal models. *J Neurooncol* **119**, 297–306.

[24] Morris Jr SM, Kepka-Lenhart D, and Chen LC (1998). Differential regulation of arginases and inducible nitric oxide synthase in murine macrophage cells. *Am J Physiol* **275**, E740-747.

[25] Sica A, Larghi P, Mancino A, Rubino L, Porta C, Totaro MG, Rimoldi M, Biswas SK, Allavena P, and Mantovani A (2008). Macrophage polarization in tumour progression. *Semin Cancer Biol* **18**, 349–355.

[26] Sindrilaru A, Peters T, Wieschalka S, Baican C, Baican A, Peter H, Hainzl A, Schatz S, Qi Y, and Schlecht A, et al (2011). An unrestrained proinflammatory M1 macrophage population induced by iron impairs wound healing in humans and mice. *J Clin Invest* **121**, 985–997.

[27] Ries CH, Cannarile MA, Hoves S, Benz J, Wartha K, Runza V, Rey-Giraud F, Pradel LP, Feuerhake F, and Klaman I, et al (2014). Targeting tumor-associated macrophages with anti-CSF-1R antibody reveals a strategy for cancer therapy. *Cancer Cell* **25**, 846–859.

[28] Burnett SH, Beus BJ, Avdiushko R, Qualls J, Kaplan AM, and Cohen DA (2006). Development of peritoneal adhesions in macrophage depleted mice. *J Surg Res* **131**, 296–301.

[29] Maes W, Deroose C, Reumers V, Krylyshkina O, Gijsbers R, Baekelandt V, Ceuppens J, Debyser Z, and Van Gool SW (2009). In vivo bioluminescence imaging in an experimental mouse model for dendritic cell based immunotherapy against malignant glioma. *J Neurooncol* **91**, 127–139.

[30] Szatmari T, Lumniczky K, Desaknai S, Trajcevski S, Hidvegi EJ, Hamada H, and Safrany G (2006). Detailed characterization of the mouse glioma 261 tumor model for experimental glioblastoma therapy. *Cancer Sci* **97**, 546–553.

[31] Zagzag D, Miller DC, Chiriboga L, Yee H, and Newcomb EW (2003). Green fluorescent protein immunohistochemistry as a novel experimental tool for the detection of glioma cell invasion in vivo. *Brain Pathol* **13**, 34–37.

[32] Gabrusiewicz K, Ellert-Miklaszewska A, Lipko M, Sielska M, Frankowska M, and Kaminska B (2011). Characteristics of the alternative phenotype of microglia/macrophages and its modulation in experimental gliomas. *PLoS One* **6**, e23902.

[33] Lawrence T and Natoli G (2011). Transcriptional regulation of macrophage polarization: enabling diversity with identity. *Nat Rev Immunol* **11**, 750–761.

[34] Sica A and Mantovani A (2012). Macrophage plasticity and polarization: in vivo veritas. *J Clin Invest* **122**, 787–795.

[35] Strachan DC, Ruffell B, Oei Y, Bissell MJ, Coussens LM, Pryer N, and Daniel D (2013). CSF1R inhibition delays cervical and mammary tumor growth in murine models by attenuating the turnover of tumor-associated macrophages and enhancing infiltration by $CD8^+$ T cells. *Oncoimmunology* **2**, e26968.

[36] Pyonteck SM, Akkari L, Schuhmacher AJ, Bowman RL, Sevenich L, Quail DF, Olson OC, Quick ML, Huse JT, and Teijeiro V, et al (2013). CSF-1R inhibition alters macrophage polarization and blocks glioma progression. *Nat Med* **19**, 1264–1272.